

## DNS OF INJECTION-INDUCED TRANSITION IN HYPERSONIC FLOW OVER POROUS SURFACES FOR TRANSPIRATION COOLING APPLICATIONS

**Adriano Cerminara**

Aerodynamics and Flight Mechanics  
 University of Southampton  
 Southampton, SO17 1BJ, UK  
 a.cerminara@soton.ac.uk

**Ralf Deiterding**

Aerodynamics and Flight Mechanics  
 University of Southampton  
 Southampton, SO17 1BJ, UK  
 r.deiterding@soton.ac.uk

**Neil Sandham**

Aerodynamics and Flight Mechanics  
 University of Southampton  
 Southampton, SO17 1BJ, UK  
 n.sandham@soton.ac.uk

### ABSTRACT

Results from Direct Numerical Simulations (DNS) of the Navier-Stokes equations are presented for the case of a Mach 5 low-enthalpy flow over a flat plate with coolant injection achieved through a row of slots. In particular, a slotted flat-plate configuration with four equally-spaced span-periodic slots has been considered, representative of a real experimental case, in which the dimension of the slots in the spanwise direction is much higher than the length in the streamwise direction. The novelty of our work consists in the analysis of the link between the wall cooling performance and the transition mechanism induced by high blowing ratios and by the growth of imposed unstable boundary-layer modes, identified from a previous linear stability analysis (LST) study. Results indicate that 2D and 3D unstable modes, pertaining to the class of first instability modes, exist in the considered laminar boundary layer, and that imposition of these modes within the boundary layer at different amplitudes leads to different states of the boundary layer, which we refer to as a perturbed state and a transitional state. As confirmed by comparison with experimental data, the different states of the boundary layer significantly affect the wall cooling performance, providing an increase of the wall heat flux that results in a reduction of the beneficial effects of cooling.

### INTRODUCTION

In hypersonic flows, where aerodynamic heating compromises the vehicle structure integrity, the film cooling technique (Fitt et al., 1985, 1994) represents a valid solution to suppress the heat loads experienced by the surface material. This technique is aimed at injecting coolant in the hot boundary layer to form a thin film of cold fluid adjacent to the wall, thus reducing the wall heat flux. We can distinguish two different injection strategies, namely effusion cooling (Wittig et al. 1996, Baldauf et al. 2001) and transpiration cooling (Meinert et al. 2001, Langener

et al. 2011). The former provides injection through localised holes, and is typically used for thermal protection of turbine blades surface, in which cooling occurs through a turbulent mixing layer. The latter, in contrast, takes advantage of the transpiration capabilities of a porous material to provide a more uniformly distributed coolant film. In a supersonic-hypersonic flow, however, the wall cooling requirement combines with the requirement of increasing the laminar run of the boundary layer, i.e. delaying transition. For this reason, injection through two-dimensional slots is in general preferred, as it reduces the 3D effects associated with hole injection (Heufer and Olivier, 2008, Keller et al. 2015, Keller and Kloker 2017). Our numerical study is aimed at evaluating the influence of boundary-layer stability with slot injection on the cooling performance. The system of the three-dimensional dimensionless governing equations for compressible multispecies flows, written in conservation form, under the assumption of constant specific heats, is given in Cartesian coordinates as

$$\frac{\partial \rho}{\partial t} + \frac{\partial \rho u_j}{\partial x_j} = 0, \quad (1)$$

$$\frac{\partial \rho u_i}{\partial t} + \frac{\partial \rho u_i u_j}{\partial x_j} = -\frac{\partial p}{\partial x_i} + \frac{1}{\text{Re}} \frac{\partial \tau_{ij}}{\partial x_j}, \quad (2)$$

$$\begin{aligned} & \frac{\partial \rho E}{\partial t} + \frac{\partial \left( \rho E + \frac{p}{\rho} \right) u_j}{\partial x_j} \\ &= \frac{1}{(\gamma - 1) \text{RePr} M^2} \frac{\partial}{\partial x_j} \left( \frac{\partial \kappa T}{\partial x_j} \right) \\ &+ \frac{1}{\gamma \text{ReSc} M^2} \frac{\partial}{\partial x_j} \left( \rho D \sum_k \frac{\partial c_k}{\partial x_j} c_{p,k} T \right) + \frac{1}{\text{Re}} \frac{\partial \tau_{ij} u_i}{\partial x_j}, \end{aligned} \quad (3)$$

$$\frac{\partial \rho c_k}{\partial t} + \frac{\partial}{\partial x_j} \left( \rho c_k u_j - \rho D \frac{\partial c_k}{\partial x_j} \right) = 0. \quad (4)$$

The terms  $\rho$ ,  $\rho u$ ,  $\rho v$ ,  $\rho w$  and  $\rho E$  are the conservative variables of the system of equations, where  $\rho$  is the density,  $u$ ,  $v$  and  $w$  are the velocity components respectively in the  $x$ -,  $y$ - and  $z$ -direction, and  $E$  is the total energy per unit mass. In the flux vectors, the terms  $p$ ,  $T$ ,  $\tau_{ij}$ , and  $\mu$  are respectively the pressure, the temperature, the components of the viscous stress tensor, and the dynamic viscosity of the flow. The non-dimensional quantities are obtained through normalisation of the dimensional variables with their freestream reference values: the velocity components are normalised with the freestream main velocity ( $U_\infty^*$ ), the density is normalised with the freestream density ( $\rho_\infty^*$ ), the viscosity is normalised with the freestream dynamic viscosity ( $\mu_\infty^*$ ), the temperature is normalised with the freestream temperature ( $T_\infty^*$ ), the total energy is normalised with the square of the freestream mean velocity ( $U_\infty^{*2}$ ), while the pressure and viscous stresses are normalised with the term  $\rho_\infty^* U_\infty^{*2}$ , related to the freestream dynamic pressure. Note that the superscript (\*) is used to denote dimensional values. The characteristic length chosen to normalise the length scales is the boundary-layer displacement thickness ( $\delta^*$ ). The time scales are normalised with respect to the fluid dynamic characteristic time ( $\delta^*/U_\infty^*$ ), based on the velocity of the undisturbed flow and on the characteristic length. The terms  $Re$ ,  $Pr$ ,  $Sc$ ,  $M$ , and  $\gamma$  are respectively the Reynolds, Prandtl, Schmidt and Mach numbers, and the ratio of specific heats ( $\gamma = c_p^*/c_v^*$ ) for the air, i.e. the dimensionless parameters of the flow. The Reynolds number is defined with respect to the boundary-layer displacement thickness of the similarity solution, as  $Re = (\rho_\infty^* U_\infty^* \delta^*)/\mu_\infty^*$ ; the Prandtl number is set to 0.72 for air, and  $\gamma$  is equal to 1.4. The Schmidt number is defined in terms of the mass diffusivity as  $Sc = \mu_\infty^*/(\rho_\infty^* D_\infty^*)$ . Wilke's rule is used to express the dynamic viscosity of the mixture, as described in Anderson (2006), and a power law is used to evaluate the single species viscosity. The thermal conductivity is then expressed in terms of the species viscosity, Prandtl number, specific heat and mole fraction through the following formula,

$$\kappa = \sum_k X_k \frac{\mu_k c_{p,k}}{\sum_l X_l \phi_{kl}}, \quad (5)$$

with the term  $\phi_{kl}$  defined as in Anderson (2006). The definition of the mixture diffusivity given in Anderson (2006) is used, in which the collision integral for the Lennard-Jones (12-6) potential for a binary mixture, and the relative coefficients, are taken from Keller et al. (2015) and Neufeld (1972). The reader is referred to Cerminara et al. (2018a) for the full system of equations, including the relations for the viscous stresses, the total energy and the equation of state. The only difference is that, as we are considering a binary mixture, the specific heat multiplying the temperature in the total energy relation, and the gas constant in the equation of state are mixture properties, which are given as  $c_v = c_1 c_{v,1} + c_2 c_{v,2}$ ,  $c_p = c_1 c_{p,1} + c_2 c_{p,2}$ , and  $R = c_p - c_v$ .

## NUMERICAL SCHEME AND SAMR FOR MULTISCALE RESOLUTION

The finite-volume method used to solve numerically the governing equations consists of a 6<sup>th</sup>-order cen-

tral differencing (CD) scheme in space for both inviscid and viscous fluxes, combined with a 6<sup>th</sup>-order weighted-essentially-non-oscillatory (WENO) scheme for shock capturing, along with a 3<sup>th</sup>-order Runge-Kutta method for time integration. The so-called WENO-CD scheme is provided with a switch function that turns on/off the shock-capturing scheme at discontinuities and in smooth flow regions, respectively. This method, originally presented by Hill and Pullin (2004) and Pantano et al. (2007) for large-eddy simulation (LES) of compressible flows, and used in several successive works for the study of shocked flows and chemically reacting mixtures (e.g. Ziegler et al. 2011, Ihme et al. 2013, 2015), has been recently improved for high-resolution DNS in hypersonic transitional flows and shock-boundary-layer interaction problems (Cerminara et al. 2018a, 2018b, 2019), and tested/validated against other DNS codes available at the University of Southampton, e.g. SBLI (De Tullio et al. 2013, Cerminara and Sandham, 2017) and OpenSBLI (Lusher et al. 2018), obtaining very good results.

As our numerical simulations concern the study of wall cooling in hypersonic boundary layers achieved via injection through a row of thin slots and a porous layer, a very important feature of our code that enables high-resolution in the very small length scales of the slot/porous injector, allowing for multiscale simulations, is represented by the structured adaptive mesh refinement (SAMR) method. This technique, described in the works of Deiterding (2005, 2011), allows consecutive higher grid refinement levels to be dynamically added in the high-gradient flow regions in a patch-wise fashion, thus providing higher numerical stability and solution accuracy in the flowfield as well as minimising the computational cost. For brevity purposes, the mathematical description of the WENO-CD scheme and the SAMR technique is avoided in the present contribution, and the reader is referred to the above mentioned works.

## PROBLEM SPECIFICATION

A simplified sketch of the generic problem under investigation is presented in figure 1. Coolant fluid is injected into a laminar hypersonic boundary layer from a slot injector. Underneath of the slots there is a volume where the fluid is of plenum conditions. These are set at the bottom boundary as the stagnation pressure ( $p_0$ ) and stagnation temperature ( $T_0$ ) in the plenum chamber. The simulations replicate the flow conditions in the experiments conducted by Hermann et al. (2018) to study film cooling capabilities in hypersonic flows. The freestream conditions correspond to  $M = 5$ ,  $Re = 12600$ ,  $T_\infty^* = 76.6$  K, and the wall temperature is fixed to the room temperature,  $T_w^* = 290$  K. The flow is initialised with the laminar boundary layer from the similarity solution, with a displacement thickness at the inlet location of  $\delta_0^* = 1$  mm, which represents our characteristic length. The inlet of the computational domain is taken at a distance of 127 mm from the plate leading edge. The coolant forms a thin film of fluid near the wall, that increases the boundary layer thickness. In these conditions, wall cooling is achieved by two mechanisms, namely the lower temperature of the film of fluid adjacent to the wall, and the decrease of the temperature gradient induced by a thicker boundary layer. However, the presence of boundary layer instabilities and the induced transition mechanism can have important effects on the wall heat flux and the cooling performance. The geometry consists of a 3D slotted flat plate with four equally-spaced span-periodic slots. The

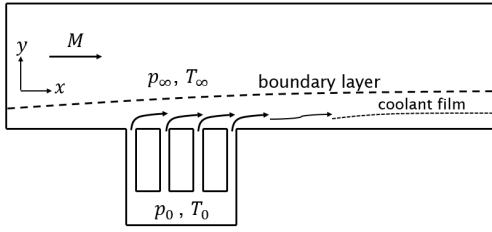


Figure 1: Sketch of coolant injection

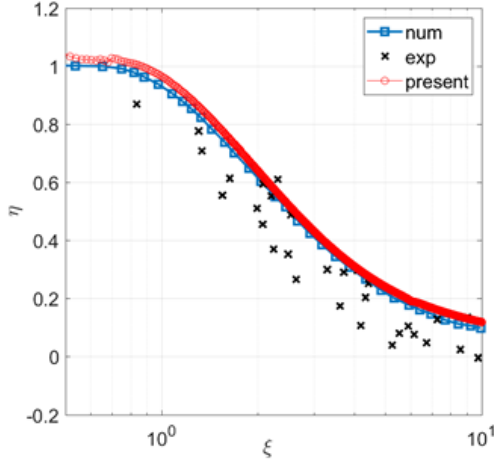


Figure 2: Cooling effectiveness for air injection

domain dimensions are  $L_x = 160$ ,  $L_y = 32$ ,  $L_z = 8$ . Each slot has an  $x$ -wise length of 0.2 mm, a  $z$ -wise length of 8 mm, which represents the computational domain width, a depth of 1.5 mm and a distance between each other of 1 mm. The base grid size is  $N_x \times N_y \times N_z = 3200 \times 384 \times 40$ . A grid study for the considered problem demonstrating the suitability of the grid size was performed and shown in Cerminara et al. (2019).

A validation test case has been considered for the cooling effectiveness against other numerical as well as experimental results available in the literature, with reference to the work of Keller et al. (2015), for both air injection and  $CO_2$  injection. Air and  $CO_2$  are injected separately in a Mach 2.6 flow, with initial laminar boundary layer obtained from the compressible similarity solution. The domain includes one slot, and injection is obtained through imposing a fixed blowing profile at the bottom boundary. For details on the set-up and flow conditions refer to Keller et al. (2015). The results of the validation study are reported in figures 2 and 3, showing the distribution of the cooling effectiveness downstream of the injection location along a normalised distance, for air and  $CO_2$  injection, respectively. As can be seen, our numerical results agree very well with both computational and experimental results reported in Keller et al. (2015).

## RESULTS

A local linear stability analysis has been performed (the LST code is described in Sansica, 2015), based on the boundary-layer profile at the position  $x = 120$ , i.e. the heat-flux sensor location, to evaluate the unstable modes present in the boundary layer and their relative role on

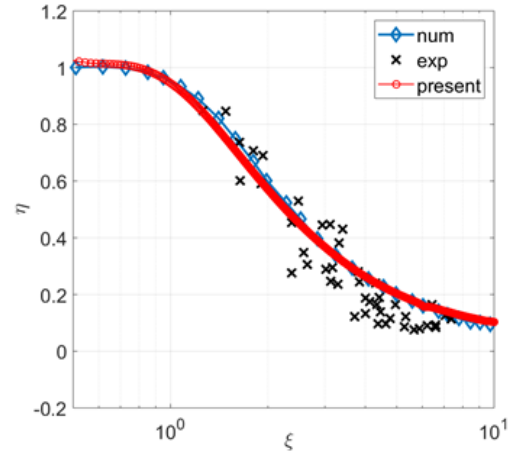


Figure 3: Cooling effectiveness for  $CO_2$  injection

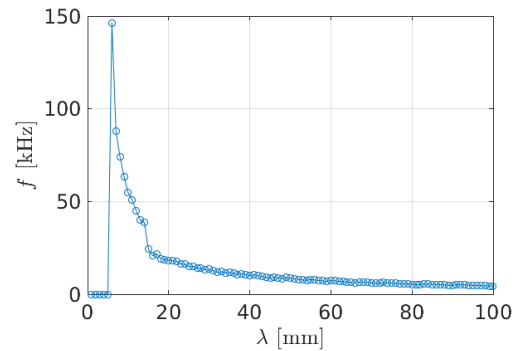


Figure 4: Frequencies of the unstable 2D modes from LST

the boundary-layer destabilization process and ultimately on the wall cooling performance. The results are plotted in figures 4 and 5 for the frequencies and the temporal growth rates of 2D modes, respectively, obtained by varying the streamwise wavenumber with a spanwise wavenumber fixed to zero. As can be seen, the region of instability involves 2D modes with a wavelength higher than about 10 mm and frequencies below 50 kHz, with the most unstable mode being characterised by a wavelength of approximately 31 mm. By performing a linear stability analysis involving also non-zero spanwise wavenumbers, it is found that the most unstable mode is a 3D mode with wavenumbers  $\alpha = 0.2$ , and  $\beta = 0.78$ , corresponding to a wavelength of 31 mm in the streamwise direction, and a wavelength of 8 mm in the spanwise direction. The temporal growth rate associated with this mode is  $\omega_i = 4.29 \times 10^{-3}$ . Hence, from LST analysis we have found that the baseflow is unstable to 2D and 3D modes corresponding to the class of first instability modes. Simulations have been performed at five different experimental values of the plenum pressure, namely i) case 1:  $p_0 = p_\infty$ ; ii) case 2:  $p_0 = 1.6p_\infty$ ; iii) case 3:  $p_0 = 1.8p_\infty$ ; iv) case 4:  $p_0 = 2.7p_\infty$ ; v) case 5:  $p_0 = 4.8p_\infty$ . Note that case 1 corresponds to the case without injection. Figures 6 and 7 show, as an example, the temperature contours in the slot-injector region for cases 2 and 5, respectively. The boundary layer appears still laminar downstream of the injection location at the lowest plenum pressure (case 2), whereas it shows a highly vortical state at the highest plenum pressure (case 5).

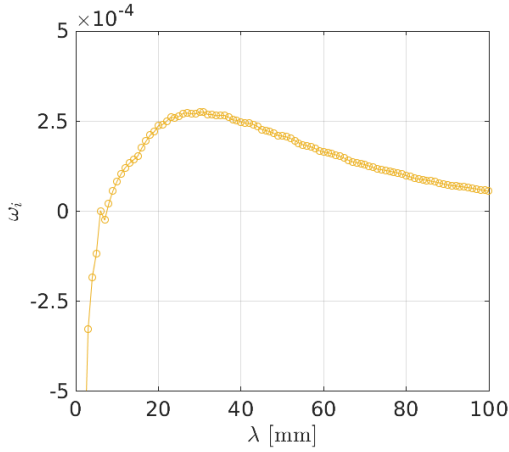


Figure 5: Temporal growth rates of 2D modes from LST

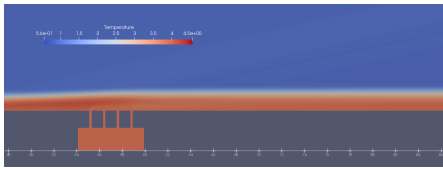


Figure 6:  $T$  field for case 2

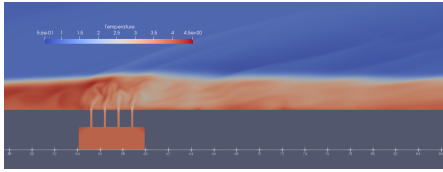


Figure 7:  $T$  field for case 5

Moreover, different sets of simulations have been performed, in which the most unstable 2D and 3D modes from LST have been inserted within the upstream boundary layer through a time-periodic blowing-suction condition imposed at the wall, using the same frequency of the unstable modes. In the first set of simulations, for all the plenum pressure conditions, the wave amplitude of each mode has been imposed equal to  $A = 5 \times 10^{-3}$ , representative of a moderate perturbation, whereas in a second set of simulations an amplitude of  $A = 2 \times 10^{-2}$  has been imposed, representative of a high perturbation. In this way we want to test the sensitivity of the boundary layer to the amplitude of the most unstable modes, and the associated effects on the wall heat flux. Figures 8 and 9 show contours of the streamwise velocity inside the boundary layer, at the height  $y = 1$ , at moderate and high amplitudes of the unstable modes, respectively, for the case without injection (case 1). In the moderate amplitude case, the evolution of the imposed (unstable) disturbances is gradual, and leads to the start of a nonlinear growth in the downstream region (note that the slots are positioned between  $x = 55$  and  $x = 60$ ). We evidence this as a perturbed state. In the high amplitude case, instead, a rapid nonlinear growth is observed, which leads to transition further downstream.

Figure 10 shows the time-averaged skin friction coefficients for both the moderate and high amplitude cases, which reveals that transition takes place for the high-

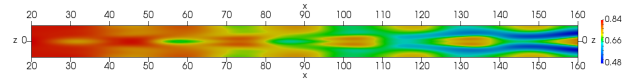


Figure 8:  $u$  inside the boundary layer ( $y = 1$ ) for the perturbed case ( $A = 5 \times 10^{-3}$ )

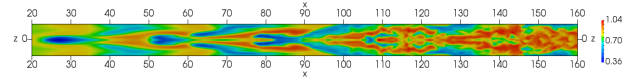


Figure 9:  $u$  inside the boundary layer ( $y = 1$ ) for the transition case ( $A = 2 \times 10^{-2}$ )

amplitude case, whereas in the perturbed case the rapid increase downstream of  $x = 80$  indicates that the boundary layer is in a pre-transitional stage.

Figure 11 shows a comparison between the experiments and the DNS in terms of the wall heat flux values at the sensor location (at  $x = 120$ ), for all the plenum pressure conditions. Note that for the moderate amplitude case, a sensitivity study with respect to the 2D and 3D most unstable modes has been made. As we can see, when considering simulations without disturbances (the ideal state), the heat flux rapidly decreases as the plenum pressure is increased, diverging from the experimental values. Whereas, when we consider the presence of the most unstable modes (2D and 3D) at a moderate amplitude, the numerical values are within the range of the measurements. When considering high disturbance amplitudes, instead, the obtained heat-flux values are significantly higher than the experimental values, which is due to the flow rapidly going through transition in this case.

Figures 12 and 13 show contours of the streamwise velocity on a  $zy$  cross section at the sensor location  $x = 120$  for case 1 (no injection) and case 5 (highest injection rate), respectively. As can be seen, in case 1, and similarly for the cases with low plenum pressure, the boundary layer at moderate disturbance amplitude appears perturbed by the 3D unstable modes, but is still in a laminar state, whereas a transitional state is achieved at the high amplitudes. In case 5, instead, transition appears to occur both at the moderate and high amplitudes, due to the high blowing ratio, and the boundary layer is significantly thicker than in the case with no injection. In the high amplitude case, however, the boundary layer is more energetic due to the enhanced mass exchange between the lower and upper layers, which results in a high velocity and temperature gradients at the wall. Figure 14 shows the time-averaged trend of the temperature inside the boundary layer near the wall ( $y = 0.1245$ ) along the streamwise direction. For the higher plenum pressure cases, the temperature assumes lower values downstream of the slot injector, but it increases further downstream with a rate that is dependent on the relative role of the internal unstable mode growth in each case. In case 5 the recover of the temperature is relatively fast, due to the flow undergoing transition. At the same time, in the latter case wall cooling benefits from the enhanced mixing, with cold flow carried towards the wall from the upper high-speed layers by vortical structures, which provides a further decrease of the heat flux. Figure 15 shows contours of the scalar representing the coolant species mass fraction within the boundary layer (at the height  $y = 1$ ), for cases 3 and 5. We observe that in case 3 (and moderate amplitude), the coolant

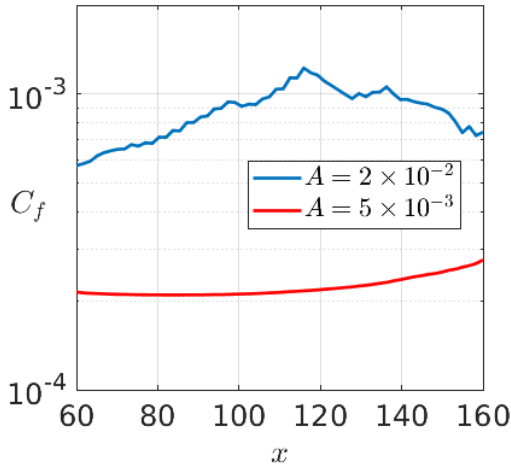


Figure 10: Time-averaged skin-friction coefficient for moderate and high amplitude disturbances

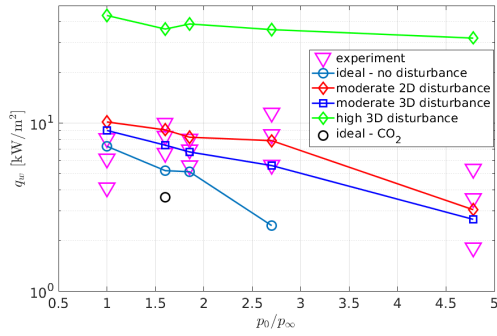


Figure 11: Comparison between measured and computed wall heat flux

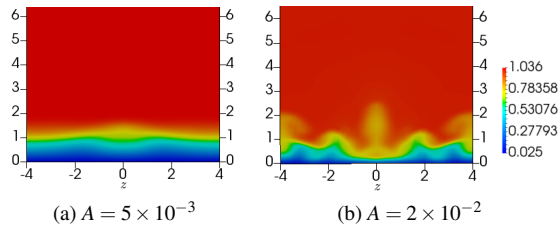


Figure 12: Streamwise velocity in the boundary layer at  $x = 120$ , for case 1 (no injection)

concentration follows the laminar flow structures formed by the evolution of the unstable mode, consistent with figure 8, whereas in case 5 the oriented structures break into a transitional state, in which mixing determines the distribution of the coolant. In particular, it is very interesting to notice that in the lower amplitude case the coolant appears to be present in high concentrations for large distances downstream. For the high disturbance amplitude, in contrast, the enhanced mixing between the lower and the upper layers of the boundary layer causes the coolant dispersion within the boundary-layer thickness, with the result that lower coolant concentrations remain in the lower layers near the wall.

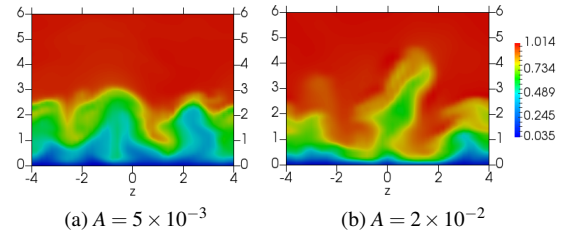


Figure 13: Streamwise velocity in the boundary layer at  $x = 120$ , for case 5

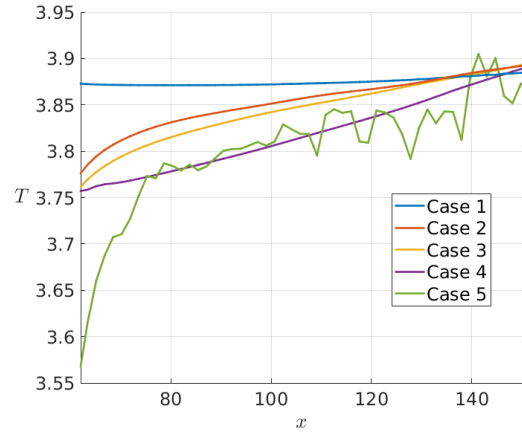


Figure 14: Time-averaged temperature profile near the wall along the centerline at moderate amplitude

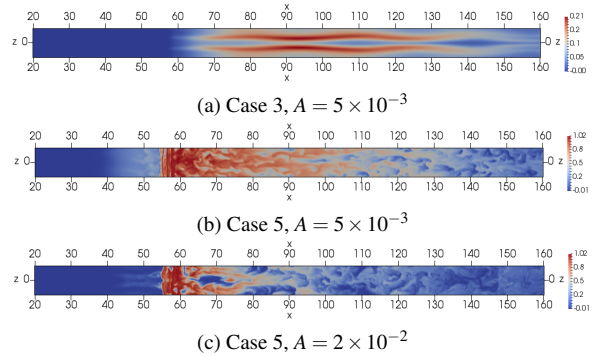


Figure 15: Contours of the coolant species within the boundary layer (at  $y = 1$ )

## CONCLUSION

DNS simulations have been run to analyse the wall cooling behaviour in hypersonic flows with span-periodic slots. Results show the relevant effects of the evolution of instability modes on their associated transition mechanism and on the wall cooling performance, demonstrating that experimental results for the wall heat flux can be explained by considering the boundary layer as in a perturbed, or pre-transitional, state. A fully transitional boundary layer induces, in contrast, significantly higher heat flux values, due to the high velocity and temperature gradients at the wall, along with the dispersion of the coolant within the upper layers of the boundary layer from an enhanced mixing.

## ACKNOWLEDGMENTS

The authors would like to acknowledge support from EPSRC (Engineering and Physical Sciences Research Council) under the Grant No. EP/P000878/1.

## REFERENCES

- Fitt, A. D., Ockendon, J. R., and Jones, T. V., "Aerodynamics of slot-film cooling: theory and experiment", *Journal of Fluid Mechanics*, 160, November 1985, pp. 15-27.
- Fitt, A. D., and Wilmott, P., "Slot film cooling - the effect of separation angle", *Acta Mechanica*, 103.1-4, 1994, pp. 79-88.
- Wittig, S., Schulz, A., Gritsch, M., and Thole, K. A., "Transonic film-cooling investigations: effects of hole shapes and orientations", American Society of Mechanical Engineers, International Gas Turbine and Aeroengine Congress and Exhibition, 96-GT-222, June 1996.
- Baldauf, S., Schulz, A., and Wittig, S., "High-resolution measurements of local heat transfer coefficients from discrete hole film cooling", *Transactions of the ASME-T-Journal of Turbomachinery*, 123.4, 2001, pp. 749-757.
- Meinert, J., Huhn, J., Serbest, E., and Haidn, O. J., "Turbulent boundary layers with foreign gas transpiration", *Journal of Spacecraft and Rockets*, 38.2, 2001, pp. 191-198.
- Langener, T., Wolfersdorf, J. V., and Steelant, J., "Experimental investigations on transpiration cooling for scramjet applications using different coolants". *AIAA Journal*, 49(7), pp. 1409-1419, 2011
- Heufer, K. A., and Olivier, H., "Experimental and numerical study of cooling gas injection in laminar supersonic flow", *AIAA Journal*, 46.11, 2008, pp. 2741-2751.
- Keller, M. A., Kloker, M. J., and Olivier, H., "Influence of cooling-gas properties on film-cooling effectiveness in supersonic flow", *Journal of Spacecraft and Rockets*, 52.5, 2015, pp. 1443-1455.
- Keller, M. A., and Kloker, M. J. "Direct Numerical Simulation of Foreign-Gas Film Cooling in Supersonic Boundary-Layer Flow", *AIAA Journal*, 55.1, 2017, pp. 99-111.
- Anderson Jr, J. D., "Hypersonic and high-temperature gas dynamics", American Institute of Aeronautics and Astronautics, 2006.
- Neufeld, P. D., Janzen, A. R., and Aziz, R. A., "Empirical equations to calculate 16 of the transport collision integrals  $\omega(l,s)^*$  for the Lennard-Jones (12-6) potential". *The Journal of Chemical Physics*, 57(3), pp. 1100-1102, 1972.
- Hill, D.J., and Pullin, D.I., Hybrid tuned center-difference-WENO method for large eddy simulations in the presence of strong shocks, *Journal of Computational Physics*, 194.2, pp. 435450, 2004.
- Pantano, C., Deiterding, R., Hill, D. J., and Pullin, D. I., A low numerical dissipation patch-based adaptive mesh refinement method for large-eddy simulation of compressible flows, *Journal of Computational Physics*, 221(1), pp. 63-87, 2007.
- Ziegler, J. L., Deiterding, R., Shepherd, J. E., and Pullin, D. I., An adaptive high-order hybrid scheme for compressive, viscous flows with detailed chemistry, *Journal of Computational Physics*, 230.20, pp. 7598-7630, 2011.
- Ihme, M., Sun, Y., and Deiterding, R., Detailed simulations of shock-bifurcation and ignition of an argon-diluted hydrogen/oxygen mixture in a shock tube, AIAA 2013-0538 Paper, 51st AIAA Aerospace Sciences Meeting including the New Horizons Forum and Aerospace Exposition, Grapevine (TX), 2013.
- Ihme, M., Sun, Y., and Deiterding R., Detailed Simulations of Weak-to-Strong Ignition of a H<sub>2</sub>/O<sub>2</sub>/Ar Mixture in Shock-Tubes, 29th International Symposium on Shock Waves 1, Springer, Cham, pp. 209-214, 2015.
- De Tullio, N., Paredes, P., Sandham, N. D., and Theofilis, V., "Laminar-turbulent transition induced by a discrete roughness element in a supersonic boundary layer". *Journal of Fluid Mechanics*, 735, 613-646, 2013.
- Cerminara, A., and Sandham, N. D., "Acoustic leading-edge receptivity for supersonic/hypersonic flows over a blunt wedge". *AIAA Journal*, Vol. 55, No. 12, pp. 4234-4244, 2017.
- Cerminara, A., Deiterding, R., and Sandham, N., "DNS of Hypersonic Flow over Porous Surfaces with a Hybrid Method", AIAA 2018-0600 Paper, AIAA Aerospace Sciences Meeting, AIAA SciTech Forum, Kissimmee (FL), 2018a.
- Cerminara, A., Deiterding, R., and Sandham, N., "Direct Numerical Simulation of Blowing in a Hypersonic Boundary Layer on a Flat Plate with Slots", AIAA 2018-3713 Paper, AIAA Fluid Dynamics Conference, Atlanta (GA), 2018b.
- Cerminara, A., Deiterding, R., and Sandham, N., "Transpiration cooling using porous material for hypersonic applications", Chapter 13 of book *Convective Heat Transfer in Porous Media*, Taylor and Francis, pp. 1-35, Apr 2019.
- Lusher, D. J., Jammy, S. P., and Sandham, N. D., "Shock-wave/boundary-layer interactions in the automatic source-code generation framework OpenSBLP". *Computers and Fluids*, 173, 17-21, 2018.
- Deiterding, R., "Construction and application of an AMR algorithm for distributed memory computers, Adaptive Mesh Refinement - Theory and Applications". *Lecture Notes in Computational Science and Engineering*, 41, Springer, pp. 361-372, 2005.
- Deiterding, R., "Block-structured adaptive mesh refinement-theory, implementation and application". *Esaim Proceedings*, Vol. 34., EDP Sciences, 2011.
- Hermann, T., Ifti, H. S., McGilvray, M., Doherty, L., and Geraets, R. P., "Mixing characteristics in a hypersonic flow around a transpiration cooled flat plate model". *International Conference on High-Speed Vehicle Science Technology*, November 2018, Moscow, Russia
- Sansica A., "Stability and Unsteadiness of Transitional Shock-Wave/Boundary-Layer Interactions in Supersonic Flows", Doctoral Thesis, University of Southampton Research Repository, 2015